Velocity field characterization of Newtonian and non-Newtonian fluids in SMX mixers using PEPT

Mihailova, Olga; O'sullivan, Denis; Ingram, Andy; Bakalis, Serafeim

DOI:
10.1016/j.cherd.2016.03.006

Document Version
Peer reviewed version

Citation for published version (Harvard):
Mihailova, O, O'sullivan, D, Ingram, A & Bakalis, S 2016, 'Velocity field characterization of Newtonian and non-Newtonian fluids in SMX mixers using PEPT', *Chemical Engineering Research and Design*. https://doi.org/10.1016/j.cherd.2016.03.006

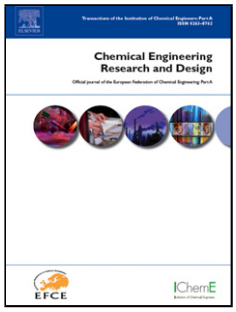

Title: Velocity Field Characterisation of Newtonian and Non-Newtonian Fluids in SMX Mixers Using PEPT

Author: Olga Mihailova Denis O'Sullivan Andy Ingram Serafim Bakalis

PII: S0263-8762(16)30011-9
DOI: http://dx.doi.org/doi:10.1016/j.cherd.2016.03.006
Reference: CHERD 2218

To appear in:

Received date: 17-8-2015
Revised date: 24-2-2016
Accepted date: 3-3-2016

Please cite this article as: Mihailova, O., O'Sullivan, D., Ingram, A., Bakalis, S.,VELOCITY FIELD CHARACTERISATION OF NEWTONIAN AND NON-NEWTONIAN FLUIDS IN SMX MIXERS USING PEPT, *Chemical Engineering Research and Design* (2016), http://dx.doi.org/10.1016/j.cherd.2016.03.006

Graphical Abstract (for review)

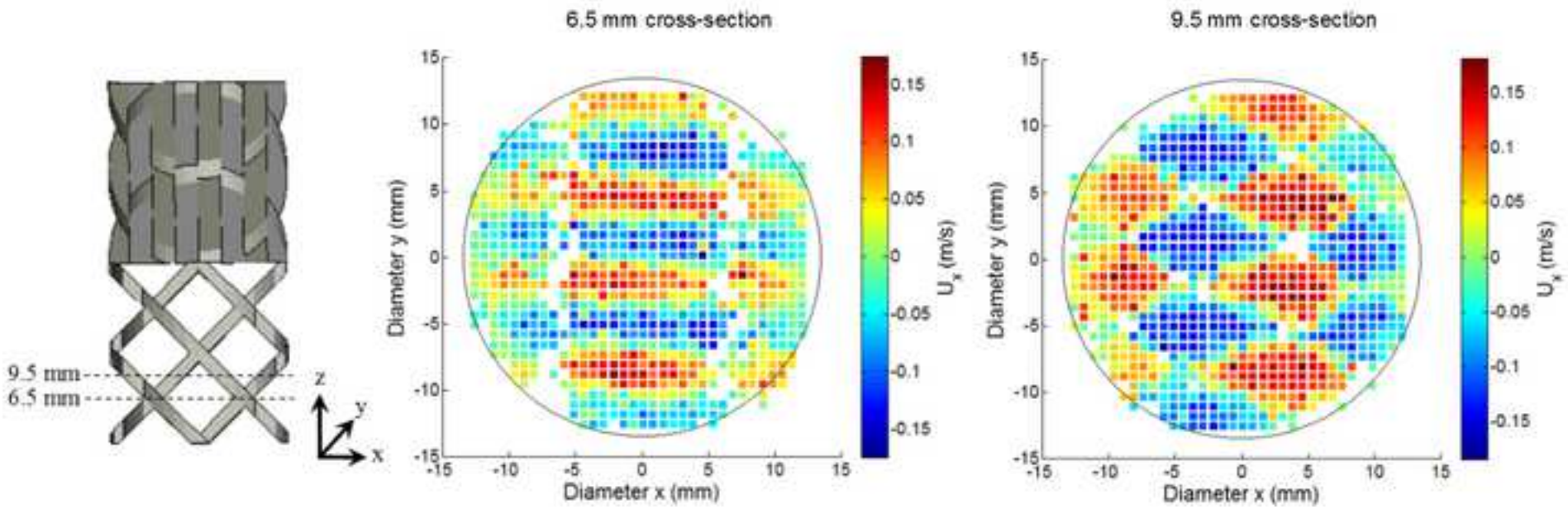

- SMX static mixers were studied using Positron emission particle tracking (PEPT)
- In the mixer the axial velocity component was not influenced by fluid rheology
- No back mixing was observed
- Radial velocities were not affected by rheology
- Radial and axial velocities were strongly influenced by the mixer geometry

VELOCITY FIELD CHARACTERISATION OF NEWTONIAN AND NON-NEWTONIAN FLUIDS IN SMX MIXERS USING PEPT

Olga Mihailova[a,b*], Denis O'Sullivan[b], Andy Ingram[a], Serafim Bakalis[a]

[a] *School of Chemical Engineering, University of Birmingham, Edgebaston, Birmingham, B15 2TT, UK*

[b] *P&G Brussels Innovation Center, Temselaan 100, 1853 Strombeek-Bever, Belgium*

Abstract

The ability to predict fluid behavior, such as velocity distribution or degree of mixing, is a critical step in designing industrial mixing processes. However, the majority of processing technologies are difficult to study using traditional approaches, due to the opacity/impermeability of the construction materials, as well as employed fluids, and geometric complexities of such systems.

The current work applies a novel technique, Positron emission particle tracking (PEPT), which allows characterization of complex systems. PEPT relies on triangulation of γ-rays emitted by a radioactive tracer particle, allowing the study of geometrically complex systems regardless of the system properties. This study compares the velocity distributions a Newtonian fluid, glycerol, and a non-Newtonian fluid, guar gum solution (0.7% w/w), flowing through 10 elements of a DN25 SMX mixer at 300 L/h.

Axial velocity remained positive throughout and no back-mixing was exhibited. The velocity components appeared to be independent of rheology, with the overall flow across 10 mixer elements resembling plug flow. Radial velocities were unimodally distributed around zero in the direction where no mixing was induced, while in the direction in which radial mixing is induced the velocity distributions were either uni- or bimodal, depending on the geometry of the cross-section.

Keywords. SMX, PEPT, Velocity, Newtonian, Non-Newtonian

* Corresponding author. *Tel*.: +44 (0) 7772953668; *Email address*: OXM186@bham.ac.uk

1. INTRODUCTION

Continuous processing presents several benefits over the traditional batch or semi-batch approaches which are predominantly used in fast moving consumer goods industries. Continuous processing allows reductions in waste and energy, as well as consumption of material, which leads to more streamlined processes and optimized processing times (Nienow et al., 1997). Many continuous processing steps involve mixing and blending of streams with different rheological properties, with the properties of the combined streams often differing to that of the inlet streams. Such processing steps are often achieved by the application of static mixers, therefore understanding and characterizing the processes occurring within static mixers is crucial for efficient process development (Meijer et al., 2012; Mihailova et al., 2015)

The current work addresses the demand for an enhanced understanding of flow patterns within industrially utilized SMX static mixers (Figure 2). SMX mixers, originally developed by Sulzer, are used in a variety of applications, including mixing miscible components (e.g. blending), combining immiscible streams (e.g. emulsification, encapsulation, etc.), as well as for processes that include a reaction step between the inlet streams (e.g. purification) (Das, 2011; Fradette et al., 2007). Furthermore, SMX mixers can be applied to multiphase processes, dispersing gases or solids through a liquid phase (Fradette et al., 2006; Laporte et al., 2015). SMX mixers are designed for laminar flow applications and rely on breaking and recombining the bulk of the inlet streams into smaller streams, using a series of channels (Paul et al., 2004). For the case of miscible fluids, such as those addressed in this study, the individual channels guide the streams to come in contact with each other, creating striations within the bulk. The

alternating geometry of the mixers induces the development of such striations across the entire cross-section of the mixer, ultimately leading to fully a mixed flow (Mihailova et al., 2015).

The majority of evaluation of such systems to date has been conducted using indirect approaches, due to the complexity and impermeability of the construction materials, such as stainless steel, and the materials flowing through the system, for example shampoo (Fradette et al., 2007; Visser and Rozendal, 1999). As a result the majority of characterization relies upon the analysis of the mixer output stream, through Particle image velocimetry (PIV) (Leschka et al., 2007), pulsed ultrasonic velocimetry (Hammoudi et al., 2008) as well as blending of immiscible materials to assess the level of dispersion at the outlet (Das et al., 2013; Fradette et al., 2006; Hammoudi et al., 2012). Moreover, the flow and mixing patterns within SMX mixers have been explored using computational fluid dynamics (CFD), where numerical simulations were used to predict the velocity fields within the boundaries of the mixer based on a series of assumptions about the underlying forces and the resulting properties of the flow (Visser and Rozendal, 1999; Zalc et al., 2002). The definition of the velocity fields further allows to seed tracer particles into the system, assessing the mixing patterns and the degree of mixing at the output (Liu et al., 2006).

Positron emission particle tracking (PEPT) offers a novel direct approach for tracking flow within systems, such as static mixers, that are not readily applicable for study using applied methods. PEPT has been demonstrated as an effective technique for the characterization of flow within kenics static mixers (Rafiee et al., 2011). Use of neutrally buoyant 200 μm radioactive tracer particles, that are sufficiently small to behave as a representative volume of the fluid, with the Stokes number below 2×10^{-5}, it is possible to trace the flow through the system of interest irrespective of the materials used in construction or the fluids flowing through the system.

The current study focuses on characterizing local velocity distributions within a 25mm SMX static mixer assembly, containing 10 mixer elements. Local velocity estimations can be achieved by analyzing the rate of displacement of individual particle passes as they travel through the mixer. This work focuses on comparing local velocity fields of two fluids with distinct rheological properties, Newtonian glycerol and Non-Newtonian shear-thinning guar gum solution (0.7% w/w), moving through the mixer assembly at 300 L/h. Understanding the effects of rheology on the flow of fluids through the mixer provides valuable insight into the dynamics of the mixer and allows superior process design, optimizing manufacturing processes which utilize SMX mixers.

2. MATERIALS AND METHODS

2.1. Materials

2.1.1. Fluids

Pure glycerol (Reagent, UK) and 0.7% w/w guar gum solution (Impexar, UK) were used for the current work. These fluids were chosen as the majority of fluids used in continuous liquid mixing processes exhibit either Newtonian (glycerol) or shear thinning (guar gum) behavior under the conditions of the flow (Singh et al., 2009) (Figure 1). The behavior of guar gum under shear was best described by the Carreau–Yasuda model (Eq. 1) (Yasuda et al., 1981),

$$\mu_{eff}(\dot{\gamma}) = \mu_{inf} + (\mu_0 - \mu_{inf})(1 + (\lambda\dot{\gamma})^a)^{\frac{n_y - 1}{a}} \quad (1)$$

Where μ_{inf} = 0.01 Pa.s, μ_0 = 5.27 Pa.s, λ = 0.76 s, n_y = 0.23 and a = 0.80. However, based on the Streiff-Jaffer correlation (Eq. 2) (Streiff et al., 1999) it is possible to determine the expected average shear rate in a static mixer based on the average velocity (V) and the diameter of the mixer (D).

$$\dot{\gamma}_{av} = \frac{64V}{D} \quad (2)$$

Under the conditions of the flow, the expected average shear rate is ~ 380 s^{-1}. As can be seen in Figure 1, for this range of shear rates it is possible to assume that the fluid behaves as a simple Power law fluid (Eq. 3), where the constants are as follows n_p = 0.32 and m = 4.50 Pa.s.

$$\mu_{eff}(\dot{\gamma}) = m\dot{\gamma}^{n_p-1} \quad (3)$$

For all models the effective viscosity (μ_{eff}) is representative of the bulk viscosity, at higher shear rates ($\dot{\gamma}$). As a Newtonian fluid glycerol maintains a constant viscosity of 1.13 Pa.s across the entire range of shear rates. For guar gum solution the shear rate at the wall was chosen for the estimation for the apparent viscosity, as it has been previously applied for similar calculations in SMX mixers (Li et al., 1997).

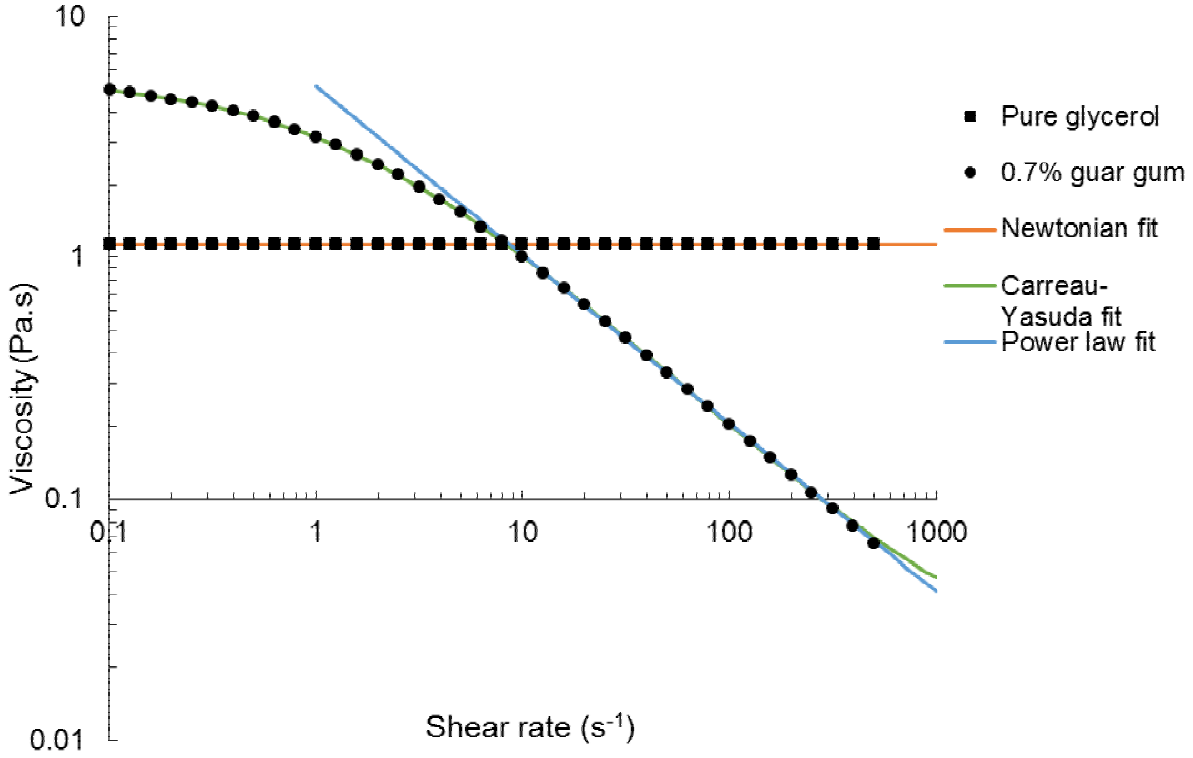

Figure 1. Effect of shear rate on the viscosity of glycerol and 0.7% w/w guar gum solution, at 22.5°C. Solid markers represent experimental data obtained using rotational rheometry. Color lines represent fluid model fits, Newtonian for glycerol (orange), and Carreau-Yasuda (green) and power law (blue) for guar gum solution.

2.1.2. SMX Mixers

For the purposes of this work SMX mixers with diameter of 25mm, or D25, were used. The SMX static mixers elements have a characteristic structure with 6 planes of blades, where each alternating plane is at 90 degrees to the preceding (Figure 2a), creating a crisscross lattice which redirects the fluids in a stretch and fold manner inducing mixing across the pipe cross-section in the direction parallel to the orientation of the blades. Each consecutive mixer element is mounted at 90 degrees to the preceding, which in turn induces mixing across the pipe cross-section but perpendicular to that in the prior element. SMX assemblies normally contain an even number of elements, to allow for the same number of elements in each orientation, to ensure balanced

mixing in every direction. For this work, the two cross-sectional planes at 6.5 mm and 9.5 mm will be considered, along with the mixer as a whole. Despite the different distribution of the mixer geometry across the cross-section (Figure 2b), the area that is unobstructed and available for the flow of the fluid remains constant. These two cross-sections illustrate how the geometry of the mixer changes along the mixer length, presenting the two extreme cases, a cross-section divided into larger section by solid walls (6.5mm) and a cross-section with smaller compartments segregated, but not isolated, by the network of mixer blades (9.5mm).

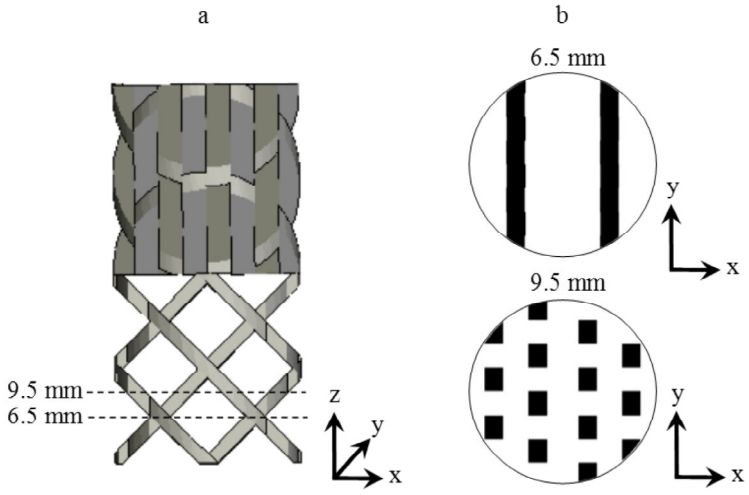

Figure 2. (a) Schematic representation of two SMX mixer elements and (b) cross-sections at 6.5 and 9.5 mm into the first mixer element.

To reduce the effect of the metal lattice on the path of the γ-rays that are emitted by the PEPT tracer particles and are used in location mapping the SMX mixers used in the current work were 3D printed in VeroClear plastic (Stratasys Ltd, USA), with the mixer blades 2 mm thick, as opposed to the stainless steel (SS) alternative typically used in industry, with the blade thickness of 1 mm. The blades were made thicker to enhance the structural integrity of the assembly. However, this reduces the voidage of the system, which in turn results in increased pressure drop

across the mixer. Through comparing pressure drop data in both SS and plastic mixers of equivalent diameters at a range of flowrates it was established that pressure drop across the 3D printed mixer is ~20 % greater than that in a SS mixer, for both fluids. This observed difference in pressure drop agrees with the expected pressure drop difference estimated using the Darcy–Weisbach equation, when accounting for the reduction of the cross-sectional area available for flow.

2.2. Methods

2.2.1. Positron emission particle tracking

Positron emission particle tracking (PEPT) has been first developed at the University of Birmingham in the early 1990s and is based on a preexisting medical technique known as positron emission tomography (PET) (Parker et al., 1993). PEPT has been successfully used in a number of studies charactering a wide range of industrial equipment, such as vertically stirred mills (Conway-Baker et al., 2002), tumbling mills (Volkwyn et al., 2011), stirred tanks (Chiti et al., 2011), as well as home appliances, such as washing machines (Mac Namara et al., 2012).

The technique relies on tracing a single radioactive particle through the system of interest. The particle spatial location is estimated through triangulation of back to back γ-rays that are emitted during radioactive decay of the fluorine-18 isotope, encapsulated in the particle, and picked up by an array of detectors, or cameras, either side of the equipment. For each location the triangulation algorithm uses of up to 100 individual γ-ray pairs, with outliers and invalid pairings removed, to provide improved location accuracy. With fluorine-18 having a half-life of less than 110 minutes the gamma emission is rapid enough to estimate the averaged particle location once every ten milliseconds and due to the application of γ-rays, that can penetrate most materials, allows using the technique on real, unmodified industrial systems. However, a balance

between the rate of displacement and the rate of location acquisition needs to be struck, to ensure reliable results. The 3D tracer location data with respect to time allows the derivation of a number of system properties, such as occupancies, concentrations, mixing efficiencies, local velocities and local shear rates (Bakalis et al., 2006).

For the current work neutrally buoyant ~200 μm tracer particles were used. A single particle was present in the flow at any given time and allowed to recirculate until the activity was lost and a new particle could be introduced. In excess of 800 individual particle passes were recorded for each set of experimental conditions, to give a high probability of detection across the entire system, sufficient to reconstruct the flow regime in the volume of the mixer element using PEPT particle locations.

2.2.2. Experimental Rig

Figure 3 below illustrates a schematic representation of the experimental rig used for the PEPT trials studying SMX mixers. 10 SMX elements were encased in a 26 mm diameter Perspex pipe and placed between the PEPT detectors, with approximately 15 cm of empty pipe on either side of the mixer within the field of view, to assess the velocity distribution within simple geometries, for technique validation (Abulencia and Theodore, 2009). The flow rate was controlled using a variable speed pump (Xylem, UK) and monitored using an inline flow meter (Krohne, USA), the fluid carrying the tracer particle was continuously recirculated around the system. Two pressure transducers (Keller AG, Switzerland) were located either side of the field of view. The temperature was not controlled, but was monitored, and throughout all trials remained within the 22.5 ± 0.5^{o}C. Laboratory scale rheological tests on a rotational rheometer

(TA Instruments, USA) using a 60 mm aluminum cone and plate geometry have shown that such temperature variations do not affect the rheological properties of the fluids significantly.

The volume of the system outside of the field of view was minimized, to reduce the time it takes for the particle to return to the field of view, as well as the volume of the carrier fluid required for the experiments, as the radioactive components within the tracer particle were observed to leech into the carrier fluid, leading to in an increase in background radiation, reducing the contrast between the tracer and the background, requiring the system to be periodically emptied and refilled with uncontaminated fluid.

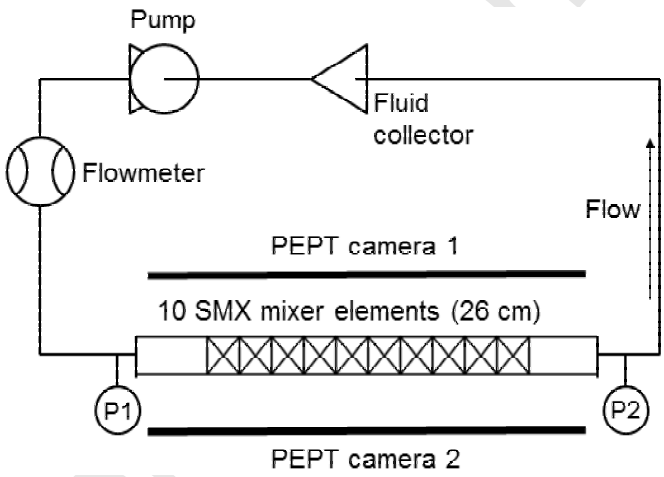

Figure 3. Schematic representation of the experimental set up

The flowrate of both fluids was maintained at 300 L/h throughout all experimental resets. This flowrate was chosen as it reflects typical industrial flowrates for such mixer diameters and while maintaining the Reynolds number for both fluids under 20, ensuring laminar flow. Laminar flow regime was defined by using the pore Reynolds number Re_p (Eq 4), as it has been previously applied for flow characterization within SMX mixers, where the mixer is treated as a

196 porous medium (Hammoudi et al., 2008; Hirech et al., 2003). For the conditions of these
197 experiments $Re_p < 15$ for glycerol and $Re_p < 11$ for guar gum.

198 $$Re_p = \frac{\rho V \tau d_p}{\varepsilon \mu_{eff}} \quad (4)$$

199 Where V is the average velocity in the empty pipe (m/s), ρ is the density (kg/m^3), τ is the
200 tortuosity (-), μ_{eff} is the viscosity (Pa.s), ε is the porosity (-) and d_p is the pore diameter (m).

201 This permitted the particle to quickly travel through the system outside the field of view,
202 while maintaining high detection count of up to 450 locations per pass through the field of view.

203 **2.2.3. Data Processing**

204 Raw binary PEPT data was processed using in-house algorithms in order to obtain the tracer
205 location in 3D space with respect to time, which allows the visualization of the entire volume of
206 the system using tracer locations. The data was then separated into individual particle passes
207 based on time between subsequent detections, where positions belonging to the same pass will
208 have a time difference in the order of milliseconds, while different particle passes will differ by
209 approximately one minute, as that is the time required for the tracer to travel though the system
210 outside of the field of view. Up to 800 particle passes were extracted per set of experimental
211 conditions. By fitting an expression to a series of points describing the particle trajectory over
212 time and taking a derivative of the expression with respect to time it is possible to determine
213 local velocity both along individual axes as well as overall (Mihailova et al., 2015). In order to
214 estimate the local velocity components U_x, U_y and U_z that represent the component in the
215 corresponding direction, a polynomial expression was fitted to a set of up to 7 particle locations,
216 with the central point of the range being the fitting point of interest, as shown in Figure 4. The

resulting expression took on a form shown in Eq 5, where the location of the particle along one of the axis (x, y or z) at a given time is determined by the particle trajectory with respect to the corresponding axis and time.

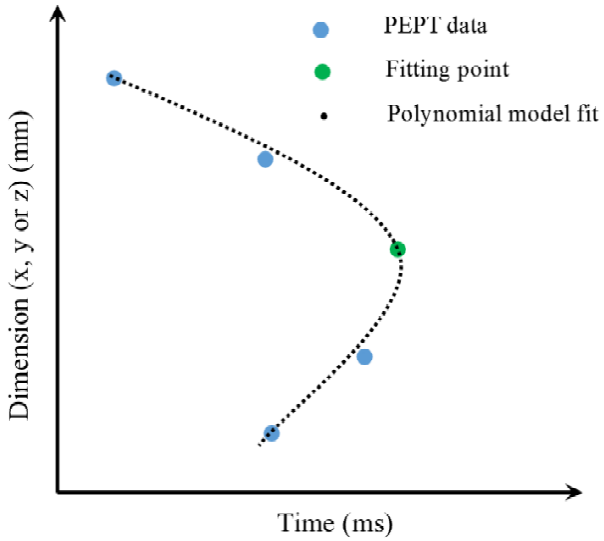

Figure 4. Schematic representation of polynomial curve fitting for local velocity estimation

By differentiating the particle location expression (Eq. 5), it is possible to obtain the rate of change of location with respect to time, i.e. velocity (Eq. 6).

$$i = a_1 t^n + a_2 t^{n-1} + \ldots + a_{n-1} t + a_n \qquad i = x, y, z \qquad (5)$$

$$U_i = \frac{di}{dt} = n a_1 t^{n-1} + (n-1) a_2 t^{n-2} + \ldots + a_{n-1} \qquad i = x, y, z \qquad (6)$$

In both expressions the exponent n was assigned values of 2 or 3, depending on whether a quadratic or a cubic function best described the pass taken by the particle between the points to which the polynomial fit was applied. Under the laminar flow conditions maintained in the experiments, the main variations to the particle trajectory were expected to originate from the changes in geometry. Based on the predicted particle velocity and the dimensions of the mixer,

the particle is not expected to change trajectory more than twice in the section of each fit, therefore a cubic expression is expected to describe any trajectory variation. However, for sections with less variation, a quadratic fit often results in less error when confirming validity of the fit by using raw data points. The decision was based on the R^2 value for both fits. Based on the average random error in both the distance and the time measurements, the error of the function derivative can reach ± 0.01 m/s, i.e. up to 5% of the average values calculated using this approach.

To enhance the resolution of the data and due to the symmetry of the mixer elements it was possible to separate the data in the mixer section into 10 discrete segments, representing one mixer element each, as shown in Figure 5. Every second element had to be rotated 90 degrees on the x-y plane, to achieve alignment. The velocity fields in first and last elements were compared to those in the remaining elements, and it was concluded that entry/exist effects were not causing discrepancies in the velocity distributions. The 10 elements were then superimposed to significantly increase the number of detections per element volume, up to 8000 particle passes, resulting in a detailed representation of a single SMX element (Figure 5).

The detailed SMX element was then separated into slices perpendicular to the z-axis (i.e. direction of the flow) allowing to visualize and assess the velocity distribution filed within the different zones of the mixer element.

Velocity distributions across the SMX mixer were assessed by comparing them to standard unimodal and bimodal distributions. Where a unimodal distribution exhibits a single mode, i.e. only a single highest values is observed. A bimodal distribution, on the other hand, is a superposition of two unimodal distributions, exhibiting two distinct maxima.

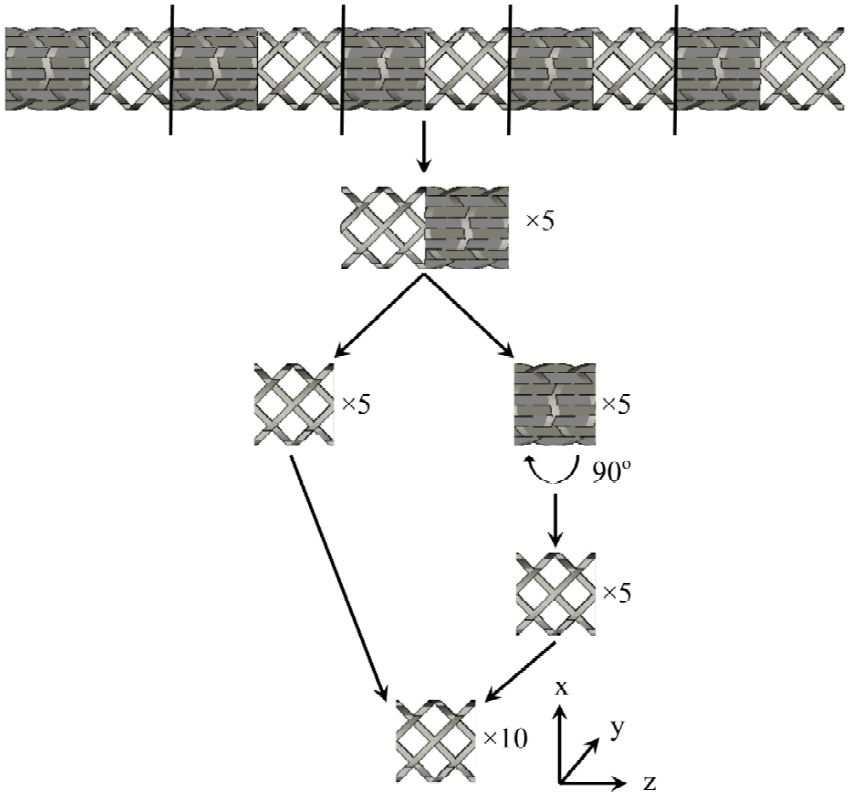

Figure 5. Schematic representation for the separation of the 10 element mixer assembly into individual elements.

The Kolmogorov-Smirnov two-sample test with a 95% confidence interval was used to assess the significance of the results. Data with $P < 0.05$ were considered statistically significant.

All of the above computational processing was conducted for both fluids using in-house developed scripts in MATLAB R2013a (MathWorks, USA).

3. RESULTS AND DISCUSSION

Based on the dramatically different geometry of the mixer cross-sections (Figure 2b) and the intricate lattice of the mixer blades, it can be expected the velocity distribution within the mixer element relies on the geometry, which is designed to redirect and alter fluid streams to induce

mixing. However, it has to be noted that depending on the specific location within the mixer element the intensity of the velocity field varies, as the walls, or blades, of the mixer geometry come together and move apart, blending the streams. In addition to the differences in the geometry of the cross-section, it is also important to consider the orientation of the mixer element, which defines the direction in which mixing is induced.

After collapsing the data from 10 mixer elements into one, the orientation of the resulting element is such, that radial velocity component U_x becomes the velocity in the direction of induced radial mixing, with the flow parallel to the mixer blade alignment, while U_y becomes the velocity perpendicular to the direction in which mixing is induced. Figure 2b illustrates the geometry of the cross-sections in resulting mixer element. It can be expected that the magnitude of the velocity field in the direction of induced mixing will be higher than that in the direction in which mixing is not actively induced.

However, when a number of elements are considered, due to the nature of the SMX mixer geometry, where each consecutive element is oriented at 90 degrees to the preceding element, the direction in which mixing is brought about by the arrangement of the mixer blades changes. This means that radial velocities U_x and U_y alternate at being the velocities in the direction of induced mixing and direction in which mixing is in each element.

Similar velocity patterns were observed both in the Newtonian and non-Newtonian fluids. Before analyzing the velocity fields at different locations within the mixer, it is important to consider how the velocity fields in the empty pipe region of the system compare to the theoretical distributions that are expected based on fluid rheology. The solid lines in Figure 6a illustrate the expected theoretical velocity profiles in the circular pipe, for the two fluids of

interest, flowing at 300 L/h, symmetrical around the center of the pipe (Abulencia and Theodore, 2009). The error bars illustrate the average deviation of the PEPT data from the model, where the error is much greater around the center of the pipe, due to low particle pass probability, as the result of the decreasing cross-sectional area with increasing distance from the pipe wall. The error is also high close to the wall, as particles rarely pass through this region, due to a boundary layer formed near the wall. Any particles entering the wall boundary layer became immobilized, remaining at the boundary, this often required the flowrate to be increased to dislodge the particle, or in extreme cases, required a full clean and reset of the system, leading to invalid passes being recorded in both situations. However, in the areas with high particle pass detection probability, the model and the experimental data are in agreement, where the experimental data points fit the corresponding models with coefficients of determination (R^2) of 0.951 and 0.946 for glycerol and guar gum solution, respectively.

While it is impossible to fit the velocity distribution within the mixer to the same models as the velocity distribution in the empty pipe, these data sets can be compared on the basis of how frequently the tracer particle exhibits a velocity within a certain range. Such distributions are shown for both glycerol and guar gum within the mixer in Figure 6b. No negative velocities were observed for either fluid, suggesting that no back mixing occurs when lateral mixing is induced. The differences in the distribution ranges of U_z were similar to the distributions observed in the empty pipe, with the velocity frequency distribution peaking at a higher value, but overall achieving lower velocities than glycerol. However, these differences were not as pronounced, suggesting that within the channels of an SMX mixer the rheological properties of the fluids maintain an effect on the axial velocity as in the empty pipe, but the internal dynamics of the mixer reduces the impact of rheology.

On average axial velocities of the two fluids were 30% greater inside the mixer than in the empty pipe region. This can be explained by the fact that inside the mixer the cross-sectional area available for flow is reduced, due to the introduction of the mixer structure. Based on the CAD files from which the mixer elements were printed, it is possible to calculate that the mixer occupies ~ 30 % of the empty pipe volume, suggesting $\varepsilon \approx 0.7$, this value is consistent across all cross-sections along the mixer length. Similar values have been previously quoted in literature, where $\varepsilon \approx 0.67$ for a D25 SMX mixer, indicating that 33 % of the pipe volume is occupied by the mixer (Theron and Sauze, 2011). As the flowrate stays the same, it can be estimated that for the expected reduction in area available for flow, the increase in the average axial velocity inside the mixer is ~ 30 % of that of the average axial velocity in the empty pipe. When comparing the glycerol velocity distributions inside and outside the mixer the increase is ~ 31 %, with the average value of axial velocity (U_z) outside the mixer of ~ 0.16 m/s and the average U_z inside the mixer of ~ 0.21 m/s, for glycerol. For the case of the guar gum solution the average velocity inside the mixer increases by ~ 30 %, with the average U_z inside and outside of the mixer of ~ 0.22 m/s and ~ 0.17 m/s respectively. Similar patterns were previously described by using ultrasound for velocity field reconstruction, where the overall shape of the profile resembled that of an empty pipe, but exhibited higher values (Hammoudi et al., 2008). Furthermore, in order to validate the porosity of the mixer, it is possible to calculate the total flowrate across any mixer cross-section using velocity maps as the ones shown in Figure 7a and 7c, where the size of each cell on the grid is 0.5mm×0.5mm. For the case of glycerol the average flowrate based on local velocity values was 287±5 L/h, while for guar gum solution the average flowrate was 292±7 L/h, which compares well to the nominal flowrate across the system determined by the flowmeter.

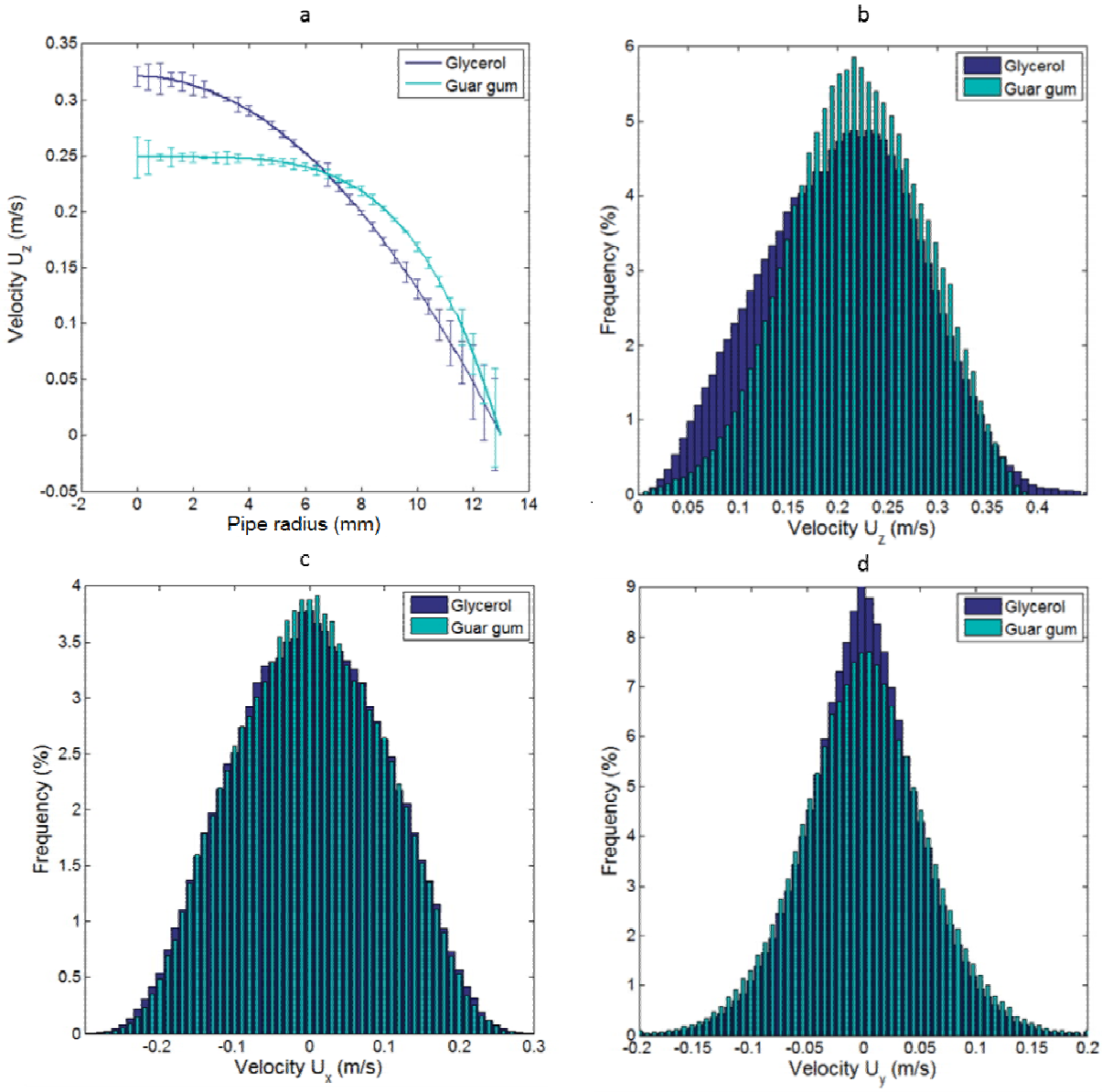

Figure 6. (a) Comparison of the empty pipe velocity profiles of glycerol and guar gum, as described by the model based on the fluid rheology. Experimental data fits illustrated by error bars. (b) Glycerol and guar gum solution velocity distribution in the direction of the flow, (U_z) inside of the mixer (c) Glycerol and guar gum solution velocity distribution in the direction of mixing, (U_x) inside of the mixer (d) Glycerol and guar gum solution velocity distribution in the direction perpendicular to the direction of mixing, (U_y) inside of the mixer. All at 300 L/h.

Within the empty pipe region any velocity components perpendicular to axial flow are equal to zero, however, within the mixer the velocity components across the x-y plane, perpendicular to the flow, become imperative to inducing the mixing. For the case of the radial velocity component in the x-direction (U_x), the direction in which radial mixing is induced in the current orientation of the mixer element, both glycerol and guar gum solution displayed a normal unimodal distribution around zero between -0.3 and 0.3 m/s, shown in Figure 6c. The velocity distribution in the y-direction (U_y), where little mixing occurs, for both fluids, is between -0.2 and 0.2 m/s, normal around zero (Figure 6d). It has to be noted, that U_x is the velocity in the direction of mixing due to the geometry, as in this orientation of the mixer element the mixer blades are parallel to the x-axis. The fluid follows the channels formed by the mixer blades, and due to the laminar nature of the flow, motion along the y-axis is not expected. Therefore, the magnitude of U_y is lower than U_x and an increase in U_y is predominantly observed at interfaces of counter-flowing fluid elements.

It has been observed that all the distributions presented in the study display lower than expected frequency counts at lower values of the U_z. This is attributed to the fact that the probability of the tracer particle entering the slow flowing regions close to the assembly walls is significantly lower than the probability of finding the particle in faster moving regions, leading to reduced event counts at lower velocities. Furthermore, when the particle does enter the boundary layers, similar limitations apply as in the empty pipe, where the tracer gets permanently embedded in the stagnant fluid regions close to the wall.

When local velocity fields are considered at cross-sections perpendicular to the flow the unimodal pattern is not consistently observed. Depending on the geometry of the cross-section (cf. Figure 2b) both unimodal and bimodal distributions can be displayed.

It was observed, that for case of the axial velocity component, U_z, the distribution at individual cross-sections matches that demonstrated when the entire mixer is considered. Unimodal distribution patterns were displayed for both fluids, irrespective of the position of the cross-sectional plane (Figure 7). Comparison of U_z values at 6.5 mm (Figure 7b) and 9.5 mm (Figure 7d) cross-sections demonstrate that velocity distributions for each fluid at these cross-sections are consistent, with the averages comparable within the space of experimental error.

As before (cf. Figure 6b), for glycerol the observed range was between 0.00 and 0.43 m/s, with the mean at 0.21 m/s, while for guar gum solution the range was between 0.00 and 0.38 m/s with the mean at 0.22 m/s, at both cross-sections and the same as when the mixer is considered as a whole and using the t-test analysis it is possible to conclude that the velocity distributions for both fluids belong to the same continuous distribution ($P > 0.05$). Figures 7a and 7c illustrate velocity maps, highlighting the effects of the geometry on the local velocity fields. The similarities in the distributions at different radial cross-sections are due to constant cross-sectional area available for flow, irrespective of the location of the cross-section (cf. Figure 2b) and a constant flowrate across each x-y-plane.

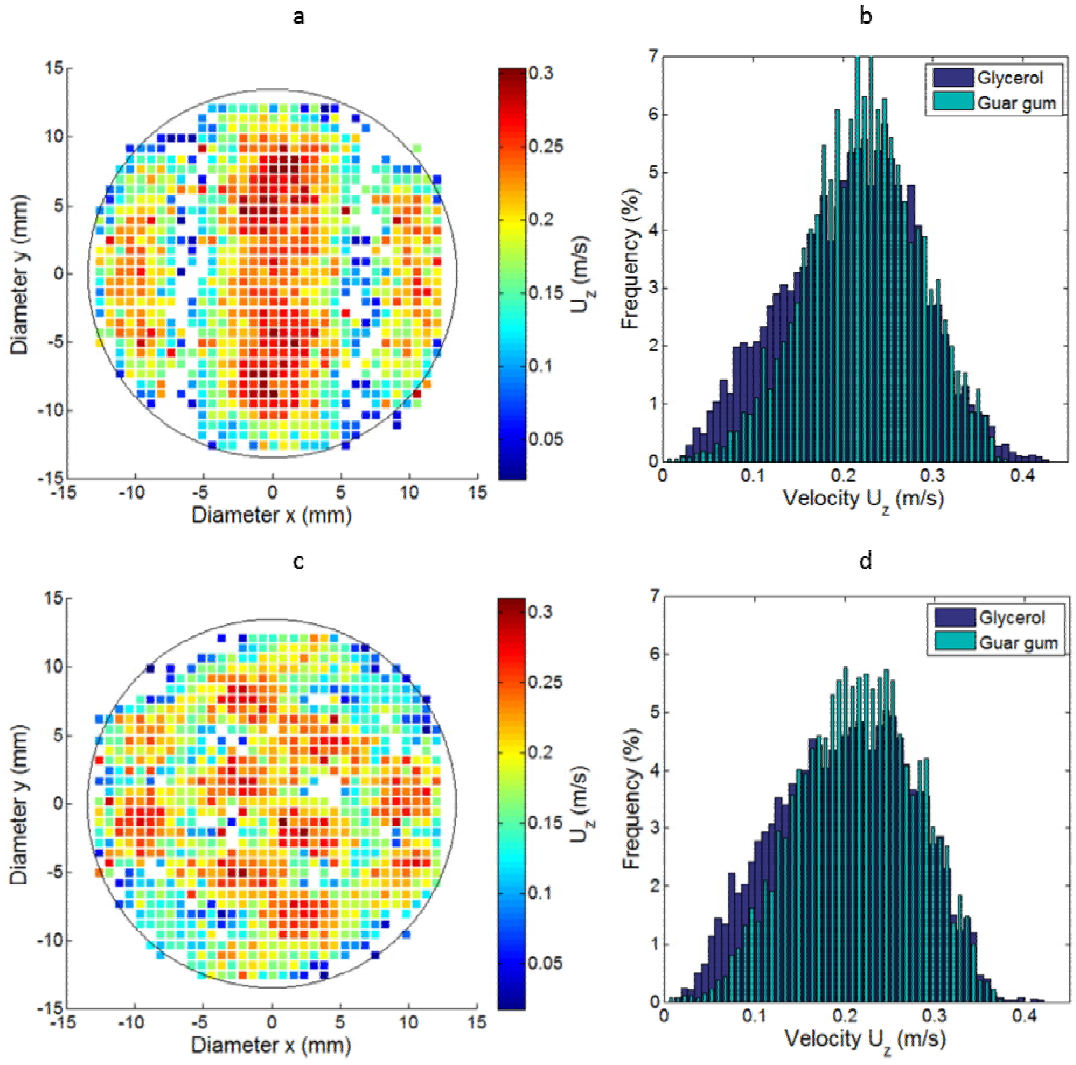

Figure 7. (a) U_z velocity map across the mixer cross-section at 6.5 mm for glycerol at 300 L/h and (b) the corresponding distributions for glycerol and guar gum solution. (c) U_z velocity map across the mixer cross-section at 9.5 mm for glycerol at 300 L/h and (d) the corresponding distributions for glycerol and guar gum solution.

Figure 8a represents the map of U_x distribution for glycerol flowing at 300 L/h across a cross-section at 6.5 mm into the SMX element, while Figure 8b illustrates the frequency of detection for different ranges of U_x at that cross-section, for both fluids. It can be seen that both distributions are unimodal around 0, while the differences in the fluid rheology do not appear to have an effect on the distribution. Conversely, Figure 8c shows the distribution of U_x at the x-y

plane 9.5 mm into the mixer element. When considering the frequency of detection plot, Figure 8d, it is clear that the distribution is bimodal, with the two maxima at -0.1 and 0.1 m/s. The difference in velocity patterns between the two cross-sections is attributed to the changing geometry of the cross-section at different points along the z-axis.

At 6.5 mm the blades of the mixer converge and the cross-section is divided into three parts, with a larger section in the middle and two smaller sections on the sides, where fluid flowing in opposite directions comes in close contact, resulting in areas where the opposing velocities cancel each other, reducing U_x, leading to a dominant peak around 0 m/s.

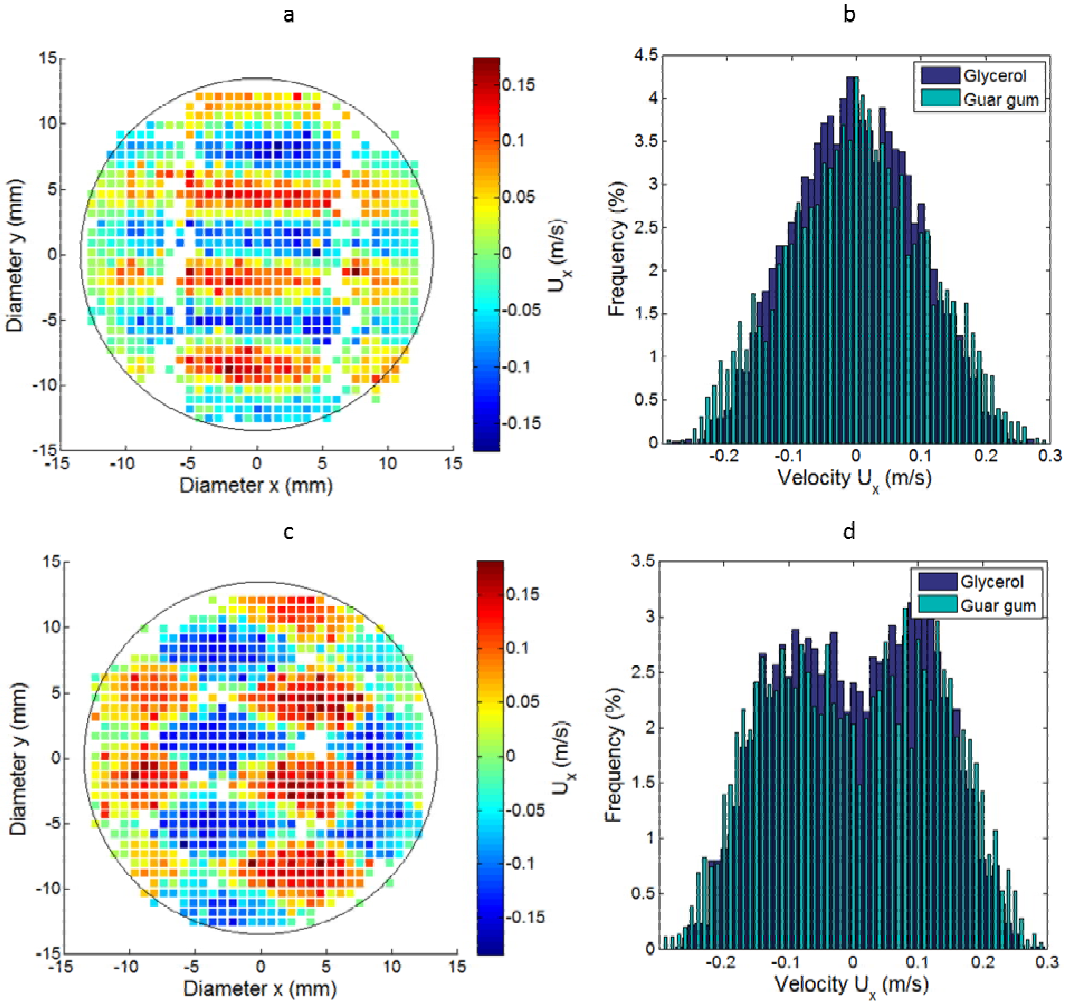

Figure 8. (a) U_x velocity field across the mixer cross-section at 6.5 mm for glycerol at 300 L/h and (b) the corresponding distributions for glycerol and guar gum solution. (c) U_x velocity field across the mixer cross-section at 9.5 mm for glycerol at 300 L/h and (d) the corresponding distributions for glycerol and guar gum solution.

Conversely, at 9.5 mm the cross-section is divided into 14 similarly sized sections, which can be clearly seen in Figure 8c as areas of opposing velocity magnitudes. This segmentation of the geometry in turn leads to a more defined division of the fluid into streams flowing in opposite directions, thus resulting in the bimodal distribution observed at 9.5 mm cross-section, as the contrasting streams do not come in contact. Such patterns of cross-section geometry are observed throughout the mixer, leading to varying velocity distribution patterns.

These velocity distribution patterns do not appear to be influenced by the rheological properties of the fluid, and the distributions for guar gum display the same patterns to those shown for glycerol (Figure 8b and 8d).

When the velocity field in the y-direction is examined (U_y), the distribution remains unimodal, irrespective of the point of the cross-section, however, the range of velocities observed varies. For glycerol flowing at 300 L/h it can be seen that at the x-y-plane at 6.5 mm depth (Figure 9b) the range is wider, between -0.2 and 0.2 m/s, while the x-y-plane at 9.5 mm depth, shown in Figure 9d, has a narrower range, between -0.15 and 0.15 m/s. The difference in the velocity range can be explained by referring back to the U_x distribution shown in Figure 8. Due to a higher fraction of the fluid moving at higher velocity in the x-direction at the depth of 9.5 mm and assuming that energy dissipated at each cross-section is the same at a constant flowrate (Hammoudi et al., 2012), the energy remaining for flow induction in the y-direction is lower, hence the narrower range of velocities observed, as U_z distribution is maintained consistent at each cross-section.

For all glycerol and guar gum solution velocity distribution pairs shown in Figures 8 and 9 it was demonstrated that the differences between the distributions are statistically insignificant ($P > 0.05$).

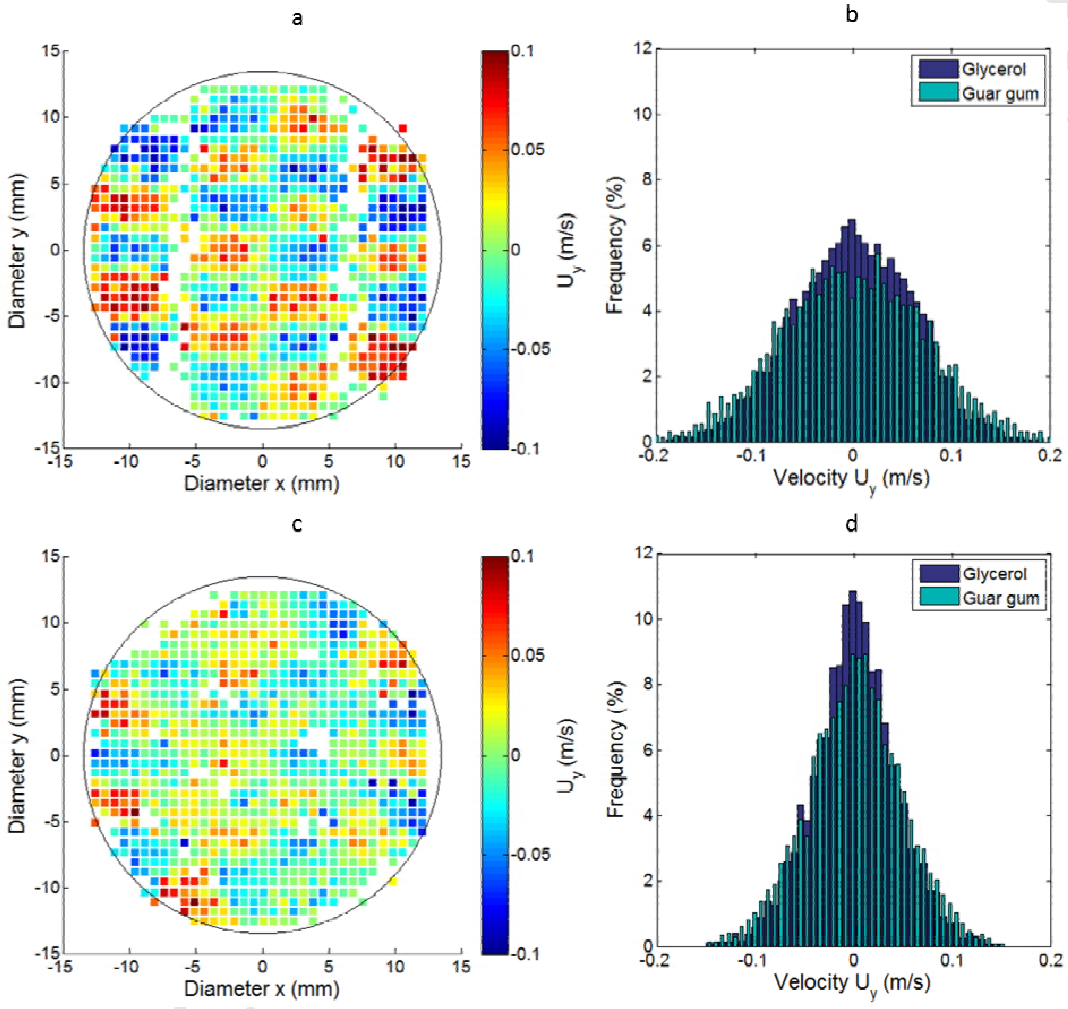

Figure 9. (a) U_y velocity field across the mixer cross-section at 6.5 mm for glycerol at 300 L/h and (b) the corresponding distributions for glycerol and guar gum solution. (c) U_y velocity field across the mixer cross-section at 9.5 mm for glycerol at 300 L/h and (d) the corresponding distributions for glycerol and guar gum solution.

By considering the residence time distributions and the total distances travelled by the tracer particles it is possible to gain further insight into the dynamics within SMX mixers. Figure 10a

illustrates the time to breakthrough for the empty pipe of the length equivalent to 10 SMX elements. It can be clearly seen that rheology has a dramatic effect on the residence time distribution, where the shear thinning guar gum solution exhibits a more plug flow behavior when compared to Newtonian glycerol, with 95% of the tracers clearing the length of the pipe in under 2100 ms, while for glycerol it takes over 3500 ms for 95% of the tracers to travel the same distance. Here, due to the laminar nature of the flow the distance travelled by the tracers is constant and equal to the length of the pipe. However, when considering the residence time distribution within the mixer itself it becomes apparent that the differences between the two fluids are less pronounced, with both exhibiting plug flow like behavior, which is a defining future of SMX static mixers as convection is induced in directions normal to the flow (Hirschberg et al., 2009) (Figure 10b). For both fluids the first tracers start emerging from the tenth mixer element at approximately 900 ms after entering at the first element, where 95% of the particles following guar gum reach the end of the last element after 1500 ms, while for the particles in glycerol it takes 1700 ms for 95% of the tracers to exit.

Due to the axial movement of the tracer particles the total distance travelled by the tracers is almost double the distance travelled in an empty pipe of the same length and diameter, specifically, the length of 10 SMX mixer elements is 260mm while the particles in both glycerol and guar gum solutions travel approximately 560mm on average (Figure 10c).

Based on these values it is possible to establish that the average total velocity, U, at which the particle travels through the mixer is equal to ~ 0.22 m/s for glycerol and ~ 0.23 m/s for guar gum solution, where these velocities are comparable to the predicted interstitial velocity, i.e. $Q/(A*\varepsilon)$.

The similarities between the local and the averaged phenomena observed for two fluids with distinct rheological properties within the SMX mixer suggests that the dynamics within the mixer are dominated by the mixer structure and are not significantly affected by the fluid rheology. This can be explained by the ongoing redirection, splitting and recombination of the flow, where the fluid does not travel sufficient distances to achieve fully developed flow after encountering an obstruction. For the dimensions of the system used in the current study the entry length within the mixer range between 1.8 mm, for more open cross-sections, of example at 6.5mm SMX depth, to 0.7 mm for cross-sections with multiple narrow channels, like those at 9.5mm SMX depth (Equation 7) (Shah and Bhatti, 1987). However, changes in the SMX geometry are perpetual and rapid along the length of the mixer, as is demonstrated by the dramatic changes in geometry between 6.5 and 9.5 mm cross-sections. Therefore it can be concluded that both fluids would exhibit plug flow like behavior, inherent of underdeveloped laminar flow, blurring the lines between Newtonian and shear-thinning fluid dynamics, with local velocity profiles indistinguishable at a constant flowrate.

$$L_e = 0.05ReD_c \quad (7)$$

These observations raise interesting questions about the mixing dynamics within SMX mixers and weather non-Newtonian rheology of the fluids being mixed affects the efficiency of mixing. It can be theorized, that under the flow conditions described, two fluids with matching apparent viscosities would mix at a comparable rate, regardless of the nature of the fluids. Here the assumption of the apparent viscosity derived from the wall shear rate could be applicable, as was shown in previous findings, where apparent viscosity derived from the wall shear rate has been successfully used to develop a universal model for pressure drop across SMX mixers for both Newtonian and non-Newtonian fluids (Li et al., 1997). Confirming such dynamics would

allow designing processes with high mixing efficiency based on the rheological properties of the fluids.

The assessment of mixing within systems as the one described above is a crucial part of the future work on SMX mixer characterization.

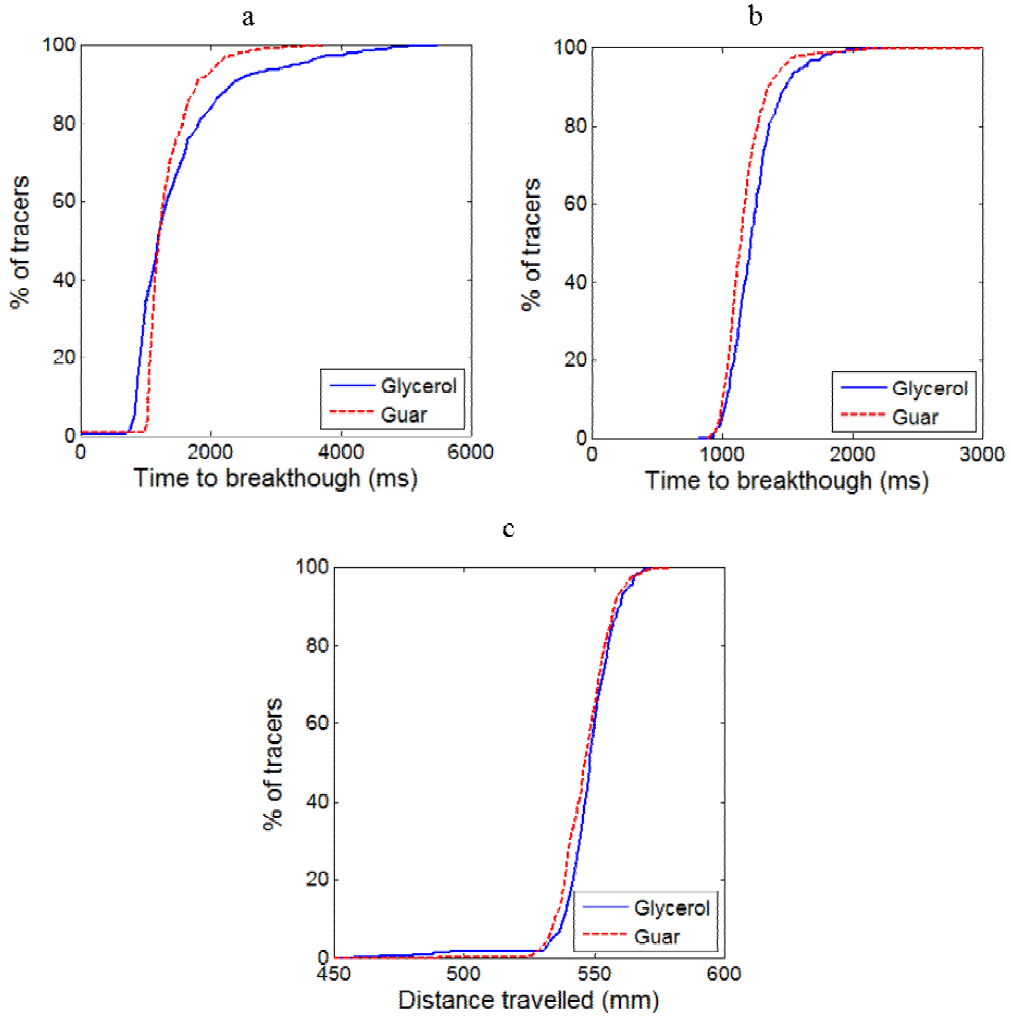

Figure 10. (a) Residence time distributions for glycerol and guar gum solution with respect to the total number of tracer particles passing through a length of empty pipe equivalent in length to 10 SMX mixer elements. (b) Residence time distributions for glycerol and guar gum solution with respect to the total number of tracer particles

passing through 10 SMX mixer elements. (c) Distributions of the total distance travelled by the tracers for glycerol and guar gum solution with respect to the total number of tracer particles passing through 10 SMX mixer elements.

4. CONCLUSIONS

The velocity distribution within SMX static mixers was assessed using PEPT and it was observed that variations in the velocity field were dependent upon location within the mixer element, predominantly differing in the direction in which mixing is induced owing to the mixer geometry.

It was shown that the velocity distribution in the direction of the flow, U_z, for the empty pipe region, was a with the theoretical velocity profile expected based on the flow conditions and the rheological properties of the fluids.

U_z distribution patterns within the mixer display similar variation between the two fluids, however the variation was not as pronounced, to such a degree that the velocities from different fluid could be attributed to the same continuous distribution, within 95% certainty. Moreover, when considering U_z distribution at specific mixer x-y-cross-sections, velocity patterns and magnitudes remain consistent, due to a constant flowrate and cross-sectional area.

Bimodal distribution patterns were exhibited by U_x, velocity in the direction of actively induced radial mixing, at locations with a high number of well-defined compartments, for example the x-y-plane 9.5 mm into the mixer element. This in turn results in a significant decrease in the magnitudes of U_y, the velocity perpendicular to the direction of induced radial mixing, when compared to cross-sections with a smaller number of larger compartments, for example the x-y-plane 6.5 mm into the mixer element.

For all three velocity components it was found that when the two fluids are considered the patterns are not significantly ($P > 0.05$) affected by the rheological properties of the fluids used in the study. This is further supported by analyzing the total residence time and total distance travelled by the tracer particles in the entire 10 element assembly, where both fluids exhibited strong plug flow behavior, uncharacteristic of fully developed laminar flow, especially for the case of Newtonian glycerol. These observations lead to the conclusion that the structure of the mixer itself has a dramatic effect on the flow, not permitting the flow to develop fully, by constantly changing the geometry of the x-y cross-section, leading to underdeveloped flow inside the mixer, comparable to plug flow. It can therefore be concluded that for fluids flowing at the same flowrate the velocity distribution would not be significantly influenced by rheology.

ACKNOWLEDGEMENTS

The authors would like to thank the Engineering, Physics and Science Research Council (EPSRC, Grant No. EP/ L015153/1) and P&G BIC for sponsoring this work. As well as Dr. Thomas Leadbeater at the School of Medical Physics at the University of Birmingham for his help in preparing the tracer particles and acquiring the PEPT data.

NOMENCLATURE

A	Cross-sectional area (m^2)
D	Mixer diameter (m)
D_c	Characteristic dimeter of pipe/channel (m)
d_p	Pore diameter (m)
L_e	Pipe/Channel entry length (m)
m	Consistency index ($Pa.s^n$)

n_p	Power Law index (-)
Q	Flowrate (m^3/s)
Re	Reynolds number
Re_p	Pore Reynolds number
t	Time (s)
U	Total velocity (m/s)
U_x	Radial velocity in the x direction (m/s)
U_y	Radial velocity in the y direction (m/s)
U_z	Axial velocity (m/s)
V	Average interstitial velocity (m/s)
x	Direction of radial flow in the direction of mixing
y	Direction of radial flow perpendicular to the direction of mixing
z	Direction of axial flow

Greek Symbols

μ_0	Viscosity at zero shear rate (Pa.s)
μ_{eff}	Effective viscosity (Pa.s)
μ_{inf}	Viscosity at infinite shear rate (Pa.s)
ε	Porosity (-)
ρ	Density (kg/m^3)
τ	Tortuosity (-)
$\dot{\gamma}$	Shear rate (1/s)

REFERENCES

Abulencia, J.P., Theodore, L., 2009. Fluid Flow for the Practicing Chemical Engineer. Wiley-Blackwell.

518 Bakalis, S., Cox, P.W., Russell, A.B., Parker, D.J., Fryer, P.J., 2006. Development and use of
519 positron emitting particle tracking (PEPT) for velocity measurements in viscous fluids in
520 pilot scale equipment. Chem. Eng. Sci. 61, 1864–1877.

521 Chiti, F., Bakalis, S., Bujalski, W., Barigou, M., Eaglesham, A., Nienow, A.W., 2011. Using
522 positron emission particle tracking (PEPT) to study the turbulent flow in a baffled vessel
523 agitated by a Rushton turbine: Improving data treatment and validation. Chem. Eng. Res.
524 Des. 89, 1947–1960.

525 Conway-Baker, J., Barley, R.W., Williams, R.A., Jia, X., Kostuch, J., McLoughlin, B., Parker,
526 D.J., 2002. Measurement of the motion of grinding media in a vertically stirred mill using
527 positron emission particle tracking (PEPT). Miner. Eng. 15, 53–59.

528 Das, M., 2011. Study of Liquid-Liquid Dispersion of High Viscosity Fluids in SMX Static Mixer
529 in the Laminar Regime.

530 Das, M.D., Hrymak, A.N., Baird, M.H.I., 2013. Laminar liquid–liquid dispersion in the SMX
531 static mixer. Chem. Eng. Sci. 101, 329–344.

532 Fradette, L., Li, H.-Z., Choplin, L., Tanguy, P., 2006. Gas/liquid dispersions with a SMX static
533 mixer in the laminar regime. Chem. Eng. Sci. 61, 3506–3518.

534 Fradette, L., Tanguy, P., Li, H.-Z., Choplin, L., 2007. Liquid/Liquid Viscous Dispersions with a
535 SMX Static Mixer. Chem. Eng. Res. Des. 85, 395–405.

536 Hammoudi, M., Legrand, J., Si-Ahmed, E.K., Salem, A., 2008. Flow analysis by pulsed
537 ultrasonic velocimetry technique in Sulzer SMX static mixer. Chem. Eng. J. 139, 562–574.

538 Hammoudi, M., SI-Ahmed, E.K., Legrand, J., 2012. Dispersed two-phase flow analysis by
539 pulsed ultrasonic velocimetry in SMX static mixer. Chem. Eng. J. 191, 463–474.

540 Hirech, K., Arhaliass, A., Legrand, J., 2003. Experimental Investigation of Flow Regimes in an
541 SMX Sulzer Static Mixer. Ind. Eng. Chem. Res. 42, 1478–1484.

542 Hirschberg, S., Koubek, R., Schöck, J., 2009. An improvement of the Sulzer SMX^{TM} static mixer
543 significantly reducing the pressure drop. Chem. Eng. Res. Des. 87, 524–532.

544 Laporte, M., Della Valle, D., Loisel, C., Marze, S., Riaublanc, A., Montillet, A., 2015.
545 Rheological properties of food foams produced by SMX static mixers. Food Hydrocoll. 43,
546 51–57.

547 Leschka, S., Thévenin, D., Zähringer, K., Lehwald, A., 2007. Fluid dynamics and mixing
548 behavior of a SMX-type static mixer. J. Vis. 10, 342–342.

549 Li, H., Fasol, C., Choplin, L., 1997. Pressure drop of Newtonian and non-Newtonian fluids
550 across a Sulzer SMX static mixer. Chem. Eng. Res. Des.

551 Liu, S., Hrymak, A., Wood, P., 2006. Laminar mixing of shear thinning fluids in a SMX static
552 mixer. Chem. Eng. Sci. 61, 1753–1759.

553 Mac Namara, C., Gabriele, A., Amador, C., Bakalis, S., 2012. Dynamics of textile motion in a
554 front-loading domestic washing machine. Chem. Eng. Sci. 75, 14–27.

555 Meijer, H.E.H., Singh, M.K., Anderson, P.D., 2012. On the performance of static mixers: A

quantitative comparison. Prog. Polym. Sci. 37, 1333–1349.

Mihailova, O., Lim, V., McCarthy, M.J., McCarthy, K.L., Bakalis, S., 2015. Laminar mixing in a SMX static mixer evaluated by positron emission particle tracking (PEPT) and magnetic resonance imaging (MRI). Chem. Eng. Sci. 137, 1014–1023.

Nienow, A., Edwards, M., Harnby, N., 1997. Mixing in the process industries. Butterworth-Heinemann.

Parker, D.J., Broadbent, C.J., Fowles, P., Hawkesworth, M.R., McNeil, P., 1993. Positron emission particle tracking - a technique for studying flow within engineering equipment. Nucl. Instruments Methods Phys. Res. Sect. A Accel. Spectrometers, Detect. Assoc. Equip. 326, 592–607.

Paul, E.L., Atieno-Obeng, V.A., Kresta, S.M., 2004. Handbook of Industrial Mixing. John Wiley & Sons.

Rafiee, M., Bakalisa, S., Fryer, P.J., Ingram, A., 2011. Study of laminar mixing in kenics static mixer by using Positron Emission Particle Tracking (PEPT). Procedia Food Sci. 1, 678–684.

Shah, R.K., Bhatti, M.S., 1987. Laminar Convection Heat Transfer in Ducts, in: Handbook of Single-Phase Convective Heat Transfer.

Singh, M.K., Anderson, P.D., Meijer, H.E.H., 2009. Understanding and Optimizing the SMX Static Mixer. Macromol. Rapid Commun. 30, 362–76.

Streiff, F.A., Jaffer, S., Schneider, G., 1999. Design and application of motionless mixer technology, in: ISMIP3, Osaka. pp. 107–114.

Theron, F., Sauze, N. Le, 2011. Comparison between three static mixers for emulsification in turbulent flow. Int. J. Multiph. Flow 37, 488–500.

Visser, J., Rozendal, P., 1999. Three-dimensional numerical simulation of flow and heat transfer in the Sulzer SMX static mixer. Chem. Eng. Sci. 54, 2491–2500.

Volkwyn, T.S., Buffler, A., Govender, I., Franzidis, J.-P., Morrison, A.J., Odo, A., van der Meulen, N.P., Vermeulen, C., 2011. Studies of the effect of tracer activity on time-averaged positron emission particle tracking measurements on tumbling mills at PEPT Cape Town. Miner. Eng. 24, 261–266.

Yasuda, K., Armstrong, R.C., Cohen, R.E., 1981. Shear flow properties of concentrated solutions of linear and star branched polystyrenes. Rheol. Acta 20, 163–178.

Zalc, J.M., Szalai, E.S., Muzzio, F.J., Jaffer, S., 2002. Characterization of flow and mixing in an SMX static mixer. AIChE J. 48, 427–436.